REGULAR ARTICLE

Impact of proximal and distal pocket site-directed mutations on the ferric/ferrous heme redox potential of yeast cytochrome *c* peroxidase

G. M. Jensen · D. B. Goodin

Abstract Cytochrome *c* peroxidase (CCP) contains a five-coordinate heme active site. The reduction potential for the ferric to ferrous couple in CCP is anomalously low and pH dependent (Eo = ∼−180 mV vs. S.H.E. at pH 7). The contribution of the protein environment to the tuning of the redox potential of this couple is evaluated using site-directed mutants of several amino acid residues in the environment of the heme. These include proximal pocket mutation of residues Asp-235, Trp-191, Phe-202, and His-175, distal pocket mutation of residues Trp-51, His-52, and Arg-48; and a heme edge mutation of Ala-147. Where unknown, the structural changes resulting from the amino acid substitution have been studied by X-ray crystallography. In most cases, ostensibly polar or charged residues are replaced by large hydrophobic groups or alternatively by Ala or Gly. These latter have been shown to generate large, solvent-filled cavities. Reduction potentials are measured as a function of pH by spectro-electrochemistry. Starting with the X-ray-derived structures of CCP and the mutants, or with predicted structures generated by molecular dynamics (MD), predictions of redox potential changes are modeled using the protein dipoles Langevin dipoles (PDLD) method. These calculations serve to model an electrostatic assessment of the redox potential change with simplified assumptions about heme iron chemistry, with the balance of the experimentally observed shifts in redox potential being thence attributed to changes in the ligand set and heme coordination chemistry, and/or other changes in the structure not directly evident in the X-ray structures (e.g., ionization states, specific roles played by solvent species, or conformationally flexible portions of the protein). Agreement between theory and experiment is good for all mutant proteins with the exception of the mutation Arg 48 to Ala, and His 52 to Ala. In the former case, the influence of phosphate buffer is adduced to account for the discrepancy, with evidence for phosphate binding in the distal pocket, and measurements made in a bis–tris propane/2-(N-morpholino)ethanesulfonic acid buffer system agree well with theory. For the latter case, an unknown structural element relevant to His-52 and/or solvent influence in the mutant akin to anion binding in the distal pocket (though lacking proof that it is, and in this case lacking a phosphate effect) manifests in this mutant. The use of exogenous (sixth) ligands in dissecting the contributions to control of redox potential is also explored as a pathway for model building.

Keywords Cytochrome *c* peroxidase · Redox potential · Site-directed mutagenesis · Heme proteins

Dedicated to Professor Akira Imamura on the occasion of his 77th birthday and published as part of the Imamura Festschrift Issue.

G. M. Jensen · D. B. Goodin
Department of Molecular Biology, The Scripps Research Institute, 10550 North Torrey Pines Road, MB8,
La Jolla, CA 92037, USA

Present Address:
G. M. Jensen (✉)
Gilead Sciences Inc., 650 Cliffside Drive,
San Dimas, CA 91773, USA
e-mail: Gerard.Jensen@gilead.com

Present Address:
D. B. Goodin
Department of Chemistry, University of California, Davis,
One Shields Avenue, Davis, CA 95616, USA

1 Introduction

Electron transfer occupies a position of central importance in biological systems. Understanding biological electron

transfer requires an understanding of the proteins and enzymes with redox active cofactors precisely tuned to optimize (both thermodynamically and kinetically) their function [46]. The electrostatic environment of such a cofactor can extend a significant control over its properties. If the cofactor incorporation into two proteins is similar (e.g., the same ligand set for a metal center), this control of redox function by the protein should be amenable to computational modeling that includes cofactor, protein, and solvent elements.

The peroxidases comprise a class of enzymes that catalyze the H_2O_2-mediated oxidation of an enormous range of biological substrates [8, 45]. The heme containing enzyme cytochrome c peroxidase (CCP) from yeast reacts with H_2O_2 to form a two-electron oxidized intermediate: compound ES. This intermediate in turn accepts electrons sequentially from two ferrous cytochromes c proteins. One oxidizing equivalent in compound ES is stored as an oxyferryl (Fe(IV)=O) heme, while the other is stored as a radical species on an amino acid side chain. In CCP, Trp-191 is preferentially oxidized to a π-cation radical to house the second oxidizing equivalent [3, 12, 22, 24, 27, 28, 48, 49]. Trp-191 in CCP is positioned as part of a so-called tryptophan-aspartate-histidine Triad (the histidine being the heme ligand) thought to contribute to the stability of the indole cation radical on tryptophan-191 [17]. The stabilization of this reaction scheme near +1 V (vs. S.H.E.) potential is reflected in the low redox potential (pH dependent Eo = ∼ −180 mV vs. S.H.E. at pH 7) of the ferric/ferrous pair stabilizing a ferric protein—compared to e.g., myoglobin, which must instead stabilize the ferrous form, and thence bind O_2 instead in an un-reactive manner. Characterization of the ferric/ferrous pair in CCP is useful to understand this space in the protein electrostatically, and as a reporter group for analysis of mutations and their electrostatic and structural consequences in an equilibrium setting, without the complexity and rapidity of the compound ES reaction. The contribution of the protein to the tuning of the redox potential of this couple has been extensively studied [5, 9, 10, 17, 31, 32, 57] and here is evaluated using site-directed mutants of several amino acid residues in the environment of the heme. These include proximal pocket mutation of residues Asp-235, Trp-191, Phe-202, and His-175; distal pocket mutation of residues Trp-51, His-52, and Arg-48; and a heme edge mutation of Ala-147. Where unknown, the structural changes resulting from the amino acid substitutions have been studied by X-ray crystallography. In most cases, ostensibly polar or charged residues are replaced by large hydrophobic groups or alternatively by Ala or Gly. These latter have been shown to generate large, solvent-filled cavities. Reduction potentials are measured as a function

of pH by spectroelectrochemistry. Starting with the X-ray-derived structures of CCP and the mutants, or with predicted structures generated by molecular dynamics, predictions of redox potential changes are modeled using the protein dipoles Langevin dipoles (PDLD) method [55]. These calculations serve to model an electrostatic assessment of the redox potential change with simplified assumptions about heme iron chemistry, with the balance of the experimentally observed shifts in redox potential being thence attributed to changes in the ligand set and heme coordination chemistry, and/or other changes in the structure not directly evident in the X-ray structures (e.g., ionization states, specific roles played by solvent species, or conformationally flexible portions of the protein). The use of exogenous (sixth) ligands in dissecting the contributions to control of redox potential is also explored.

2 Methods

2.1 CCP expression and purification from *Escherichia coli*

Wild-type and mutants (R48A, W51A, W51F, H52A, H52Q, A147Y, H175G, W191G, W191S, and F202Y) were constructed by oligonucleotide site-directed mutagenesis of single-strand DNA containing uracil as described previously [17]. Expression of wild-type and mutant proteins from *E. coli* BL21(D23) using the plasmid PT7CCP, purification, and reconstitution with heme was carried out as described previously [13, 16]. Molar absorptivities of the Soret absorption band were determined by pyridine hemochromogen assay [42] and were used to calculate protein concentrations from UV–Vis absorption spectra. The R48A and H52A mutant proteins were produced for this study; the others were available in the laboratory from previously published work. Relevant literature for the mutants utilized here can be found for W51F [16], W191G [13–15, 39–41], H175G [18, 20, 21, 36, 38, 52], R48A [19, 43], A147Y [56], and F202Y [4]. Wild-type CCP from PT7CCP in our laboratory is that with Met-Lys-Thr (and thus sometimes called MKT CCP) at the N-Terminus and containing Ile-53 and Gly-152. "Real" wild-type CCP (lacking the MKT peptide and with Thr-53 and Asp-152) was purified from *Saccharomyces cerevisiae* using the same purification methods. For H175G, purified reconstituted protein was crystallized twice against distilled water and stored as a crystal suspension at 77 K. For H175G, the extinction coefficient was determined for the 280 nm band because of variability (with pH and temperature) in the intensity and energy of the Soret band.

2.2 X-ray crystallographic analysis

Single crystals of CCP mutant proteins W51A and H52A were grown from 25% 2-methyl-2,4-pentanediol (MPD) by vapor diffusion [54]. Proteins crystallized in sitting drops with approximately 0.17 mM enzyme, 15–80 mM potassium phosphate, pH 6, and 10% MPD equilibrated against 25% MPD. X-ray diffraction data were collected at 15 °C using Cu Kα radiation from the rotating anode of a Rigaku X-ray generator and a Siemens area detector. Data were processed using the Xengen suite of programs [23]. Data were analyzed by difference Fourier techniques using the Scripps XtalView software [37]. $|F_{mutant}| - |F_{wt}|$ difference Fourier maps ("Difference Maps") were created for each mutant against the CCP (MKT) structure 1CCA (Protein Data Bank (PDB)) [17]. Models were built using XtalView and refined using repeated cycles of manual adjustment with positional B-factor refinements using the program X-PLOR [2]. For refined or partly refined structures, electron density difference Fourier maps $(2|Fo| - |Fc|)$ or "omit" maps $(|Fo| - |Fc|)$ are likewise calculated. For experiments to examine azide binding, and the generation of $|F_{ligand}| - |F_{empty}|$ difference Fourier maps, crystals were soaked at least 1 h in a mother liquor containing 10 mM Sodium Azide adjusted to pH 6 with H_3PO_4 in 28% MPD. Other relevant PDB structure entries include 1CCK (F202Y), 1CCC (D235A), 1CCE and 1CCG (H175G), 1CMQ and 1CMT (W191G), 1DJ1 (R48A), and 3CCX (A147Y).

2.3 Spectroelectrochemistry

Reducing titrations were performed anaerobically using a method adapted from those previously reported [6, 17, 50]. A 3-mL solution of approximately 5 μM CCP in buffer containing 1 mM methyl viologen and ∼1 μM of one or more of the following (depending on the observed potential of the protein): phenosafranin, Tris(ethylenediamine) cobalt(III) chloride, or 5,5′,7-indigotrisulfonic acid potassium as redox mediator was sealed in an air tight Pyrex cuvette (custom built by Rayotek Scientific, San Diego, CA) and continuously flushed with a stream of scrubbed nitrogen (a nitrogen scrubbing tower was constructed which contains 0.012 g/L 3,6 diaminoacridine HCl, 0.13 g/ L methyl viologen hydrate, 18.6 g/L Na_2H_2EDTA* $2H_2O$, 2.2 g/L NaH_2PO_4 $*2H_2O$ and 3.8 g/L Na_2HPO_4 (pH ∼ 6) and where integrity is confirmed by noting the maintenance of a green hue under white light illumination). The cell was equipped with a gold foil working electrode attached by epoxy to the cuvette wall, and this foil was scrubbed with acid and an emery board between uses; a platinum wire counter electrode; and a silver/silver chloride reference electrode. The latter two electrodes were separated from the solution by a double salt bridge, and the potential of the silver/silver chloride electrode was calibrated against a standard calomel electrode. The spectrophotometer (Hewlett-Packard 8452A), potentiostat (Princeton Applied Research Model 363), and temperature monitor were interfaced to a personal computer that controlled the automated reductive titrations (as per [17]). To prevent binding of O_2 to the reduced CCP, and to help maintain anaerobic conditions, all buffers were degassed and flushed with scrubbed N_2 before use [17]. The methyl viologen mediator also conveniently affords removal of trace O_2. To operate the cell, all components less the CCP were placed in the cell, and small amounts of reduced methyl viologen were produced electrochemically, and this procedure was repeated until reduced methyl viologen could be maintained for >30 min. The CCP sample was then introduced through an injection port for the titration. For each point, a small quantity (∼250 pmol) of methyl viologen was reduced at the working electrode by transiently applying 8 μA across the gold and platinum electrodes, followed by an equilibration period. After the potential had stabilized (∼5–15 min), the optical spectrum and the potential between the gold and the silver/silver chloride electrodes were measured. Midpoint potentials were determined from the Nernst equation by least-squares fitting of the absorbance at 438 nm versus the measured potential corrected to the standard hydrogen electrode (SHE). The Nernst slope for CCP and mutant- or ligand-bound variants reported in this study was 53.2 ± 12.1 mV (mean ± standard deviation). The wavelength for detection was adjusted as appropriate for the different mutants and ligand states. For WT CCP and mutant samples, the pH was controlled by dissolving the crystals in different mixtures of monobasic and dibasic potassium phosphate buffer, with the total concentration of buffer kept <100 mM or with a mixture of bis–tris propane (1,3-bis(tris(hydroxymethyl)methylamino)propane) (BTP) and 2-(N-morpholino)ethanesulfonic acid (MES) where the total of both buffers (BTP/MES) was <100 mM. For the H175G/Im sample, imidazole was added to the dissolved crystals at a concentration which resulted in a 20-mM concentration in the potentiometric cuvette. For the H175G/Im/N_3^- sample, sodium azide was added to the WT CCP or H175G/Im solutions so that the final concentration of N_3^- was 10 mM. For H175G, the bis-aquo species was somewhat unstable, with evidence of electrode fouling; in contrast, H175G/Im was well behaved, akin to the WT CCP.

2.4 Electrostatic calculations

Electrostatic calculations of heme oxidation/reduction were performed using the program POLARIS and the protein dipoles Langevin dipoles (PDLD) method [35, 55]. The

PDLD method has been applied to study the redox properties of heme in cytochrome c [5, 7, 33], of photosynthetic reaction centers [44], of iron-sulfur proteins [29, 30, 34, 51], of the tryptophan cation radical of CCP [1, 28], among many others. In each of these cases, some type of electrostatic representation (partial charges) for the cofactors within the proteins were derived from either ab initio or semi-empirical methods.

The PDLD calculations were carried out using an IBM RS6000 implementation of the program POLARIS [28, 35]. The redox active prosthetic group was defined to be region I and was in this case the protoporphyrin IX moiety. The protein was truncated by a sphere of radius r_2 about the centroid of region I, and the non-region I protein atoms within this radius define region II. In the PDLD method, solvent water was modeled microscopically by a grid of orientable, but positionally fixed Langevin dipoles. This approach is still computationally facile, is straightforward, and does not require the computational expense or experimental knowledge of solvent structure of more sophisticated methods (e.g., [26]). While these more sophisticated methods can certainly provide more accurate results, the size of the system and paucity of knowledge of solvent structure preclude their use here, making the PDLD approach ideal. The Langevin dipole grid, region III, was generated within a sphere of radius r_L centered again about the cluster region I centroid. In all cases $r_L \geq r_2$. For these calculations r_2 was 22 Å. Variation of r_2 to 18 or 25 Å did not significantly alter the calculated $\Delta\Delta V$ values. The Langevin system (region III) was further radially divided into an inner and outer region, the radius of the inner region being 12 Å. The Langevin dipole grid spacing was 1 and 3 Å in the inner and outer portions of region III, respectively. Solvent water beyond region III was modeled macroscopically as a continuum dielectric (region IV) using a Born expression and a dielectric constant of 80.

Starting with the X-ray-derived structures, crystallographically identified water O atoms were deleted. H atoms are added using standard bond lengths and angles. Where choices of H-atom placement were not obvious (e.g., a side chain OH group or histidine imidazole), the effects of varying these orientations on the calculations were examined and minimum energy positions were chosen. The protonation scheme for His-52 was such that $N\delta$-$H\delta$ faces Asn-82. For protein atoms and the porphyrin standard atomic partial charges, van der Waal's radii, and isotropic polarizabilities are used [35]. For the porphyrin, partial charges for the oxidized and reduced states for region I atoms were simplified following Churg and Warshel [5], and the net positive charge of the ferric state of the porphyrin was modeled as being $+0.25$ on each pyrrole nitrogen. Langevin dipoles were deleted at grid points

where the distance to any protein atom is less than the sum of the atomic van der Waal's radius and 1.4 Å.

The PDLD model calculates the electrostatic contribution, ΔV, of the protein and solvent surrounding the redox active prosthetic group to the free energy difference of the oxidized and reduced states of the redox couple. ΔV is therefore a solvation energy for the reduction. ΔV is the sum of four terms, $\Delta VQ\mu$, $\Delta VQ\alpha$, ΔVL, and ΔVB, which are, respectively, the interaction of the region I atoms with the fixed partial charges of the protein atoms, the induced dipoles of the protein atoms arising from atomic polarizabilities, the Langevin dipole grid, and the continuum dielectric. $\Delta VQ\alpha$ was produced following self-consistent iteration in the fields determined by protein atoms. Solvent water was modeled by orientable dipoles on a grid defined by a Langevin-Debye type equation. Orientation of the grid dipoles is carried out iteratively and is defined by the electric field resulting from protein partial charges, cofactor charges, and induced protein dipoles. ΔVL is the energy of interaction of the cofactor with the field defined by the solvent dipoles. For myoglobin, theoretical methods were identical, but used 1MBD (Sperm Whale) as a starting coordinate set, and the mutants at V68 (V68E, V68D, and V68N) were built from 1MBD using the program Insight (BIOSYM Technologies Inc. (now Accelrys), San Diego, CA) factoring in the reported absence of substantial structural consequences of these mutations from NMR work [53].

All calculations have been checked for convergence with respect to (a) averaging over multiple Langevin grid positions and (b) iteration to achieve the self-consistent protein polarization field and Langevin dipole orientations. For CCP, Arg-48 is given a total charge of $+1$ and Asp-235 is given a total charge of -1. All other residues, the ferrous heme, and charged moieties at the surface of the proteins (heme propionates, residues such as aspartate, glutamate, arginine, lysine) are modeled as neutral [28, 29].

The free energy, ΔG, for the reduction of a redox cofactor is the sum of the intrinsic energy of reduction of that group and the solvation energy (see e.g. [5]). While the latter is approximated by the PDLD method, the former is not in this case calculated, and therefore, only differences in redox potential due to differences in the solvation energy ($\Delta\Delta V$) are modeled. In the present case, given the presumed similarity of the structural environment of a given mutant of CCP to the native structure, $\Delta\Delta V$ is likely to result from the relatively subtle differences in the electrostatics of the two environments. Redox potential changes were obtained by using $\Delta\Delta V$ for two proteins and the conversion factor 23.06 calories/mV. Molecular dynamics (MD) was also applied for one mutation (H52A, where a larger potential shift was seen experimentally), starting with the X-ray structures and using the program POLARIS

(see [28, 29]) in order to simulate averaging over dynamically sampled states in both redox forms. MD is limited to atoms lying within a sphere of radius 12 Å, centered at the heme centroid. In addition, during MD, Cartesian constraints are applied at the Asp-235 Oε, the heme liganding His-175 Nδ, and Trp-191 Nε atoms. These constraints take the form of isotropic atomic harmonic potentials whose minima are at the crystallographic atomic positions and whose force constants (k) are 150 kcal/Å². MD was run for 25 psec at 300 K. PDLD calculations were carried out on 50 MD structures taken at 0.5 psec intervals. The results were averaged together with a $t = 0$ value to yield MD-averaged values of ΔV.

3 Results and discussion

Figure 1 shows views of the heme environment of CCP and the principal amino acid residues that occupy the proximal (containing the histidine ligand to the heme) and distal (containing the active site) pockets. Results of spectroelectrochemical titrations are shown in Fig. 2a through g. Figure 3 shows a sample plot of the change in absorbance at 438 nm and a good fit to the Nernst equation for the same data, and Fig. 4 shows a sample set of UV–Vis absorption data for the titration (H52A, pH 6.5) exhibiting clean isosbestic points. Data for CCP of native sequence (Fig. 2a) reveal a pH-dependent midpoint potential essentially identical to that reported previously [17]. Values of midpoint potential measured in phosphate buffers corresponding to the data in Fig. 2a through g and extrapolated to pH 7 are shown in Table 1. There is only a small shift in the extrapolated midpoint potential between the MKT and "real" wild-type native proteins. Data for mutants for

D235 have already been presented by Goodin and McRee [17], and somewhat large shifts were observed, as recapitulated for D235A in Table 1. For the mutant H52A (Fig. 2b), the measured potential is markedly lower, and the pH dependence has apparently been lost; this results in a relatively large shift at pH 6. At pH 7, H52A CCP has a midpoint potential ∼50 mV lower than native CCP. H52Q, also shown in Fig. 2b, gives an essentially identical result. W191G CCP (Fig. 2c) reveals a midpoint potential within 10 mV of native CCP, though there is a bit more variability in the pH-dependent data. Data for W191S also appear to overlay with data for W191G CCP. Figure 2d reveals an upward shift in potential for the mutant R48A. The pH dependence appears to be the same as that for native CCP, but the potential for R48A in phosphate buffer is ∼20 mV more positive than native CCP. Figure 2e shows data for W51A and reveals a potential also within 10 mV of native CCP; a single datum for W51F is also in the same range. The pH dependence of the W51A midpoint potential—though not quite linear—is not wholly dissimilar from that of native CCP. The mutations A147Y and F202Y are, to the degree the data are available, not different from native CCP. A147Y effectively blocks large molecule access to the δ-meso heme edge of CCP [56], while F202Y was an attempt to engineer a hydroxyl group to act as a potential hydrogen bond to Asp 235 [4]. These mutants are not discussed further.

For mutant proteins whose structures had not been characterized at the time this work was carried out—specifically the distal pocket mutants H52A and W51A—X-ray structure data were generated. Figure 5 shows an Omit Map for the partly refined structure of the H52A mutant. The map clearly shows the loss of the imidazole side chain, minor changes in position of Arg-48 and

Fig. 1 Cross-eyed stereo pair view of the active site of cytochrome *c* peroxidase. Shown are the principal proximal and distal (active) site amino acids, the heme, and the locations of Langevin dipoles from one of the dipole grids utilized in the PDLD calculations
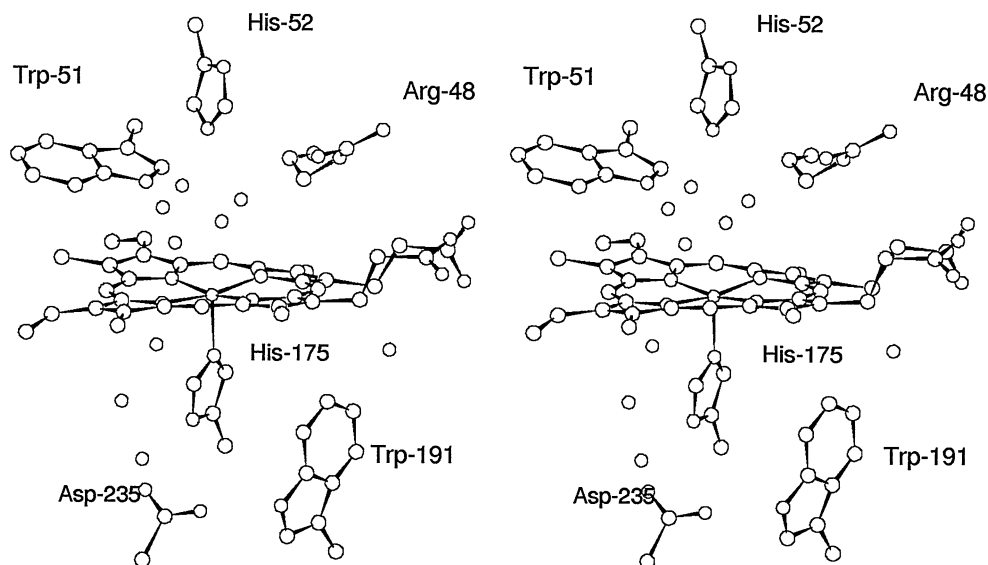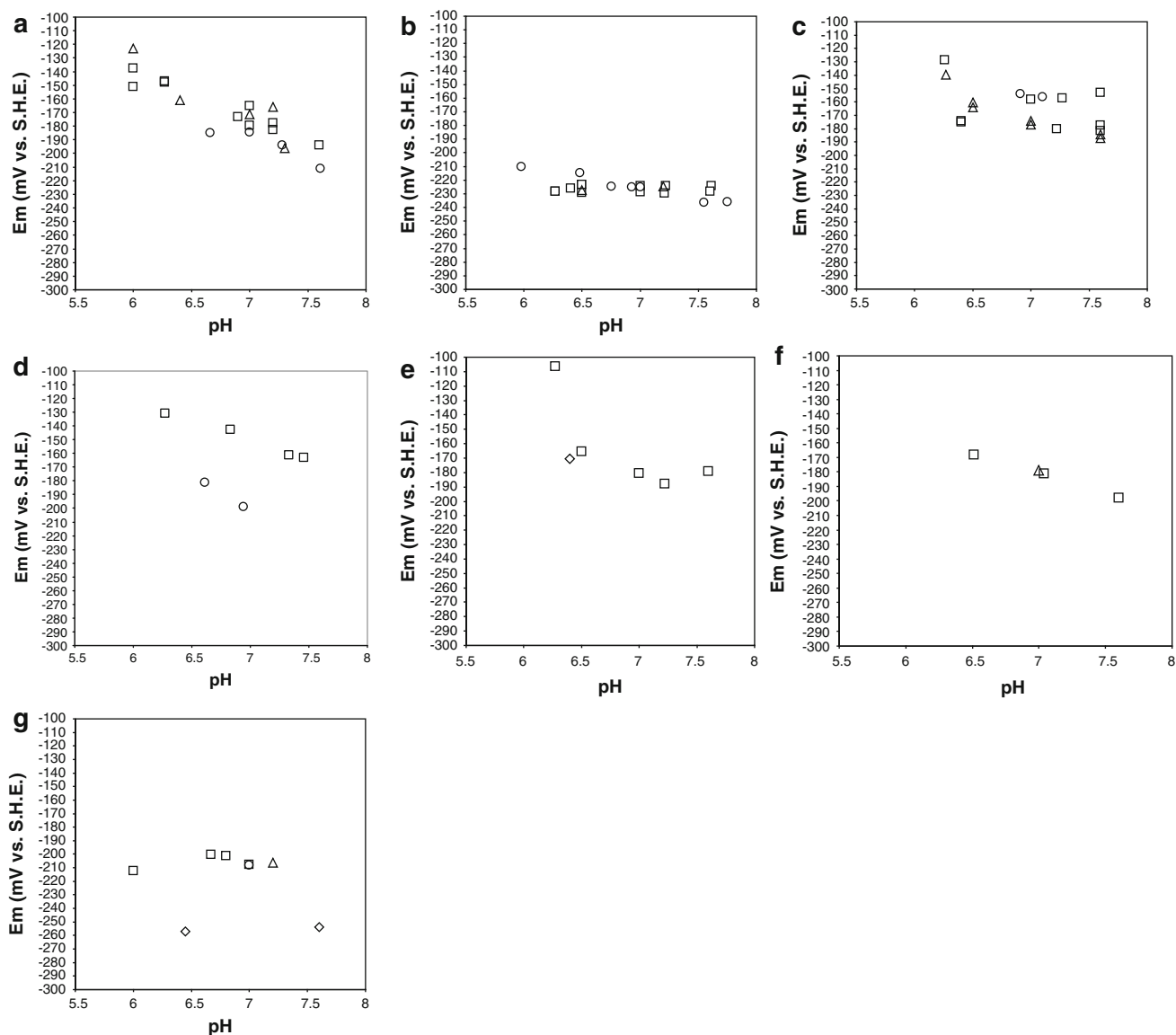
Fig. 2 a The midpoint potential for the ferric/ferrous redox couple as a function of pH for recombinant wild-type cytochrome *c* peroxidase in phosphate buffer (*triangles*); wild-type cytochrome *c* peroxidase in phosphate buffer (*circles*); and wild-type cytochrome *c* peroxidase in BTP/MES buffer (*squares*). b The midpoint potential for the ferric/ferrous redox couple as a function of pH for the mutant H52A cytochrome *c* peroxidase in phosphate buffer (*squares*); the mutant H52Q cytochrome *c* peroxidase in phosphate buffer (*triangles*); and the mutant H52A cytochrome *c* peroxidase in BTP/MES buffer (*circles*). c The midpoint potential for the ferric/ferrous redox couple as a function of pH for the mutant W191G cytochrome *c* peroxidase in phosphate buffer (*squares*); the mutant W191S cytochrome *c* peroxidase in phosphate buffer (*triangles*); and the mutant W191G cytochrome *c* peroxidase in BTP/MES buffer (*circles*). d The midpoint potential for the ferric/ferrous redox couple as a function of pH for the mutant R48A cytochrome *c* peroxidase in

phosphate buffer (*squares*); and the mutant R48A cytochrome *c* peroxidase in BTP/MES buffer (*circles*). e The midpoint potential for the ferric/ferrous redox couple as a function of pH for the mutant W51A cytochrome *c* peroxidase in phosphate buffer (*squares*); and the mutant W51F cytochrome *c* peroxidase in phosphate buffer (*diamond*). f The midpoint potential for the ferric/ferrous redox couple as a function of pH for the mutant A147Y cytochrome *c* peroxidase in phosphate buffer (*squares*); and the mutant F202Y cytochrome *c* peroxidase in phosphate buffer (*triangle*). g The midpoint potential for the ferric/ferrous redox couple as a function of pH for azide-bound wild-type cytochrome *c* peroxidase in phosphate buffer (*squares*); for azide-bound recombinant wild-type cytochrome *c* peroxidase in phosphate buffer (*triangle*); the azide-bound mutant W191G cytochrome *c* peroxidase in phosphate buffer (*circle*); and the fluoride-bound wild-type cytochrome *c* peroxidase in phosphate buffer (*diamonds*)

Trp-51, and minor changes in the area of the heme iron. Thus, the mutation results in a cavity slightly smaller (by collapse of the Arg-48 and Trp-51 side chains) than the

original imidazole moiety. Figure 6 shows a polypeptide trace of the partly refined H52A structure overlayed with the native CCP structure; the changes are confined locally
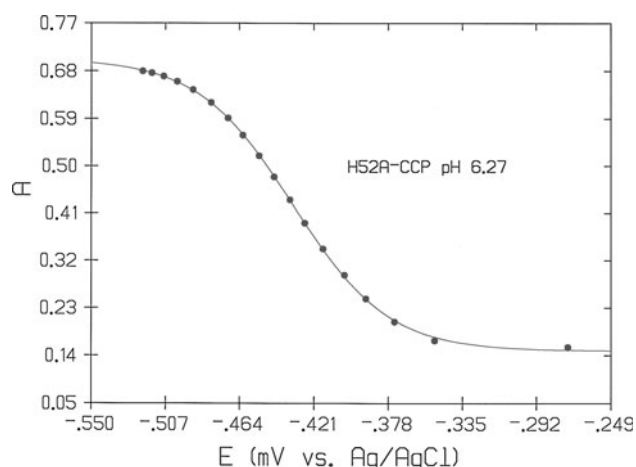
Fig. 3 Absorbance changes at 438 nm during the reductive titration of H52A CCP at pH 6.27 in phosphate buffer and fit to the Nernst equation
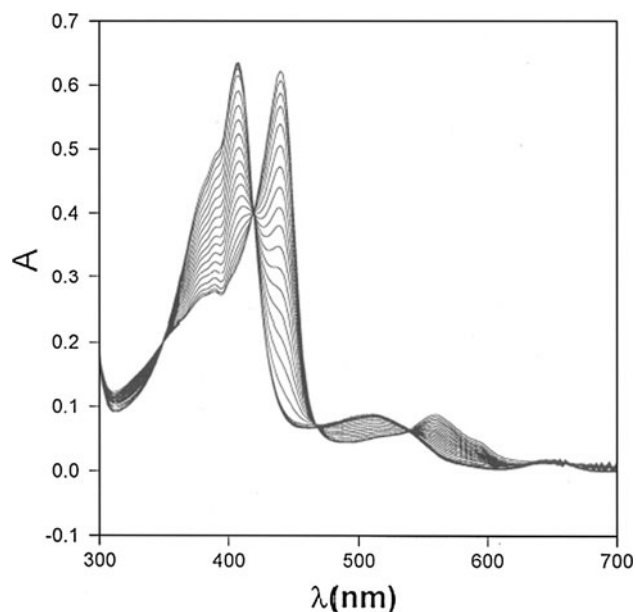

Fig. 4 UV-Vis spectral overlay during potentiometric titration of H52A CCP at pH 6.5

with the exception of some movement of polypeptide chain well distal to the heme. A difference map is shown in Fig. 7 for W51A. Again, evidence for the change is to a solvent-filled cavity created by the conversion of the indole side chain to the alanine methyl group. The published D235A, W191G, and R48A X-ray-derived structures also reveal well-characterized cavities with minimal collateral protein rearrangement. From the available structural data, we assume that to a first approximation, any change in redox midpoint potential observed on mutation for the ferric/ferrous couple will be the result of the loss of any polar or charge–charge interaction from the altered amino

acid, and the net result of the protein and solvent rearrangement attendant to the change.

Calculations using the PDLD method are presented in Table 2, and predicted shifts in midpoint potential for the ferric/ferrous pair for CCP and selected mutants are shown in Table 1. We compare results for phosphate-buffered protein measurements with the theoretically calculated shifts in potential. For D235A CCP, a -2.6 kcal/mole shift in ΔV is obtained; this is the net result of the loss of the anionic charge—which contributes a large value to $\Delta V Q\mu$, ~ 65 kcal/mole, and with resulting attenuation by solvent and changes to protein structure and polarization results in the observed shift in ΔV. Good agreement with the measured potential shift—a positive shift of 94.6 mV from experiment and 112.7 mV from the calculation—is obtained. Thus, the majority of the shift measured can be accounted for by the simple electrostatic model employed here, though there is no question that the nature of the liganding His-175 must be altered by the loss of the interaction with the charged Asp-235 (see discussion in [17]). For W51A, a small shift of 0.4 kcal/mole is evidenced (Table 2) in ΔV; this is attributed to the loss of the ~ 6 kcal/mole contribution of the Trp-51 moiety, principally the polar indole which in native CCP "points" to the heme iron (via indole Nε1 and Hε1). Agreement with the redox potential shift is good (shift of -8 mV in the experiment, and -17 mV in the calculation). For W191G, the replacement of the indole for the solvent filled cavity is calculated to give a small change in ΔV (-0.8 kcal/mole), and agreement with experiment is again good though the calculation is somewhat higher ($+8$ mV from experiment, $+35$ mV from the calculation). For R48A, the loss of the cationic charge in the distal pocket corresponds to a large change in $\Delta V Q\mu$ (~ -45 kcal/mole), and again, the PDLD model attenuates this loss of charge via the small protein structural rearrangements, protein polarity, and solvent. From the published X-ray structure [19], a water-filled cavity is created with this mutation with no significant structural perturbation outside of the distal pocket, and with a small shift in the position of His-52. The resulting calculated ΔV is 1.1 kcal/mole. The predicted potential shift of -48 mV is at odds with that measured in the phosphate buffer system at $+23$ mV. The result is also at odds with the intuitive aspect of a charge–charge interaction between the Arg-48 side chain and the ferric heme; thus, some physics is missing from the model or unanticipated in the experiment. To calibrate the model for semi-buried charge groups—we have thus far seen in this study good agreement for D235A but poor agreement with R48A—we examined some mutants of sperm whale myoglobin (Mb) published by Gray and co-workers [53]. Tables 1 and 2 show results for the same heme redox couple in Mb and the mutants V68N, V68E, and V68N [53]. The difference in

Table 1 Measured and calculated redox potentials at pH 7

Protein	Buffer system	Em, pH 7 (mV vs. S.H.E.)	ΔE_o relative to wild type	pH dependence[b]	Calc. ΔE_o
Wild-type cytochrome c peroxidase	Potassium phosphate	−172.6	0.0	Yes	
Wild-type cytochrome c peroxidase	Bis–tris propane/2-(N-morpholino)ethanesulfonic acid	−177.0	−4.4	Yes	
MKT cytochrome c peroxidase	Potassium phosphate	−189.7	−17.1	Yes	
D235A cytochrome c peroxidase[a]	Potassium phosphate	−78.0	94.6	Yes	112.7
W51A cytochrome c peroxidase	Potassium phosphate	−180.9	−8.3	Yes	−17.3
W191S cytochrome c peroxidase	Potassium phosphate	−171.7	1.0	Yes	
W191G cytochrome c peroxidase	Potassium phosphate	−164.5	8.1	Yes	34.7
W191G cytochrome c peroxidase	Bis–tris propane/2-(N-morpholino)ethanesulfonic acid	−154.9	17.7	Yes	34.7
R48A cytochrome c peroxidase	Potassium phosphate	−150.2	22.5	Yes	−47.7
R48A cytochrome c peroxidase	Bis–tris propane/2-(N-morpholino)ethanesulfonic acid	−202.3	−29.7	Yes	−47.7
H52Q cytochrome c peroxidase	Potassium phosphate	−226.4	−53.7	No	
H52A cytochrome c peroxidase	Potassium phosphate	−226.4	−53.7	No	91.1
H52A cytochrome c peroxidase	Bis–tris propane/2-(N-morpholino)ethanesulfonic acid	−225.8	−53.2	No	91.1
F202Y cytochrome c peroxidase	Potassium phosphate	−178.7	−6.1	Yes	
A147Y cytochrome c peroxidase	Potassium phosphate	−181.1	−8.5	Yes	
Wild-type cytochrome c peroxidase	Potassium phosphate + sodium azide	−202.3	−29.7	No	
W191G cytochrome c peroxidase	Potassium phosphate (pH 7.2) + sodium azide	−206.2	−33.6	No	
Wild-type cytochrome c peroxidase	Potassium phosphate + sodium fluoride	−255.5	−82.9	No	
Myoglobin	[53][c]	59	0.0	Yes	
V68N′ Myoglobin	[53][c]	−24	−83.0	Yes	−56.4
V68E Myoglobin	[53][c]	−137	−196.0	Yes	−199.5
V68D Myoglobin	[53][c]	−132	−191.0	Yes	−173.5

[a] Goodin and McRee [17]

[b] A yes implies that a given mutant approximately replicates the pH dependence seen in CCP [17] or Mb [53]. There is no assumption that CCP or Mb shares the same mechanistic origin for pH dependence of the redox potential

[c] Varadarajan et al. [53]

the midpoint potential of Mb and CCP is qualitatively reproduced, but much exaggerated, and as noted previously, the PDLD methodology we employ is best utilized for relatively small changes to similar settings. However, agreement between experiment and theory between native Mb and the mutants is well represented in the calculations: −83 mV versus −56 mV for V68N; −196 mV versus −200 mV for V68E; and −191 mV versus −173 mV for V68D; for experiment and theory, respectively. Thus, the PDLD method is well able to account accurately for "charge deletion" types of mutants in this setting. (We note that the agreement is based on electrostatic effects alone, with no element of ligation of the heme iron with one of the carboxylates included in the model). The origin of the discrepancy in R48A is explored further in the next section. For H52A, the loss of the polar imidazole and the minor rearrangement in the distal pocket result in a net change in ΔV of −1.8 kcal/mole. This leads to a prediction of a shift of +91.1 mV vs. an observed shift of −53 mV.

The calculation utilized the partly refined structure determined for H52A and the published structure of MKT CCP. Often, improved results can be obtained by averaging results obtained from the starting structures obtained by molecular dynamics simulations [28, 29]. Figure 8 shows the results of ΔV for CCP and H52A CCP over 25 ps of MD. The average shift in ΔV is now −2.1 kcal/mole, not much different from that using the single structure. The origin of the discrepancy between theory and experiment in H52A is also taken up below.

CCP studies have commonly involved phosphate buffer; as shown in studies of H175G CCP [20, 21], phosphate—a relatively small anion—may play some structural role in the distal pocket under some conditions. A BTP/MES buffer system was developed and utilized to explore this effect where it might exist. Figure 2a, b, c, and d explores the use of BTP/MES in place of phosphate buffer. As shown in Table 1, there is essentially no buffer effect in wild-type CCP. For W191G, the effect is also small; this
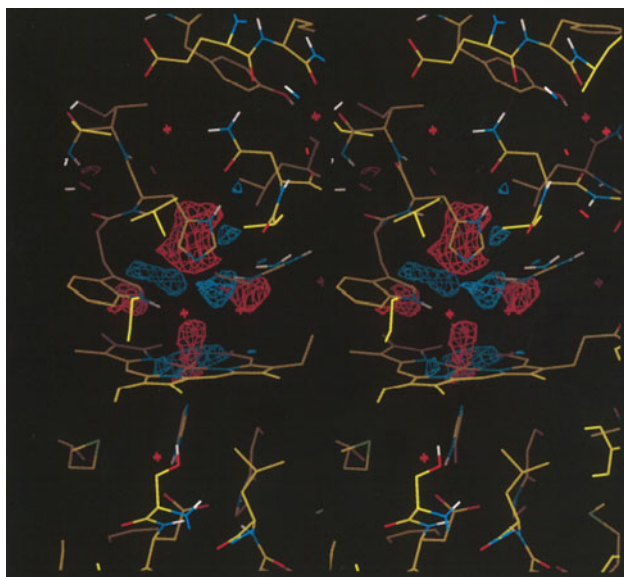
Fig. 5 Stereo omit map of H52A cytochrome *c* peroxidase. Electron density contours are shown for 2 sigma (negative 2σ, *red*; positive 2σ, *blue*). Position 52 was modeled as glycine, and $|Fo| - |Fc|$ maps were constructed after five cycles of positional refinement and three cycles of B factor refinement in X-PLOR [2]
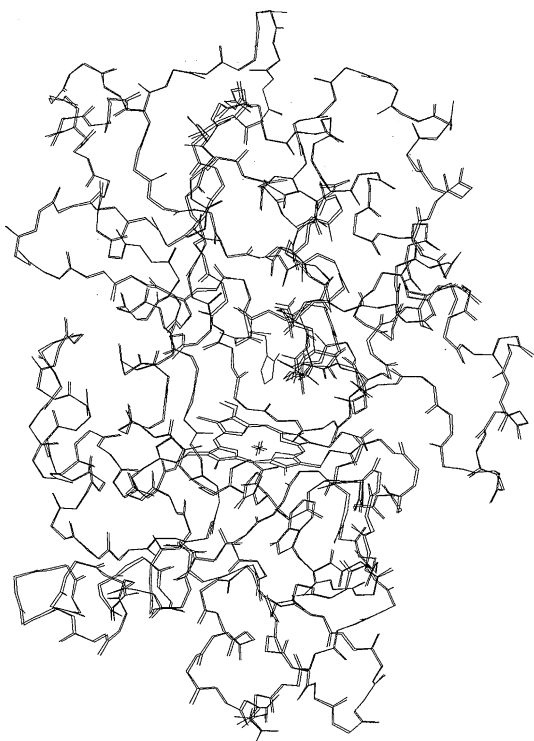

Fig. 7 $|F_{mutant}| - |F_{native}$ (MKT)$|$ difference Fourier map for W51A cytochrome *c* peroxidase. The *red* density represents a contour of -3σ, and the *blue* density represents a contour of $+3\sigma$. The map is superposed on the structure of native CCP (MKT)

Fig. 6 Polypeptide traces of the overlayed structures of H52A and native (MKT) CCP

was to be expected as this cavity is well known to support cation binding [14, 40, 41]. For R48A, however, a substantial buffer effect is noted; the potential goes from a
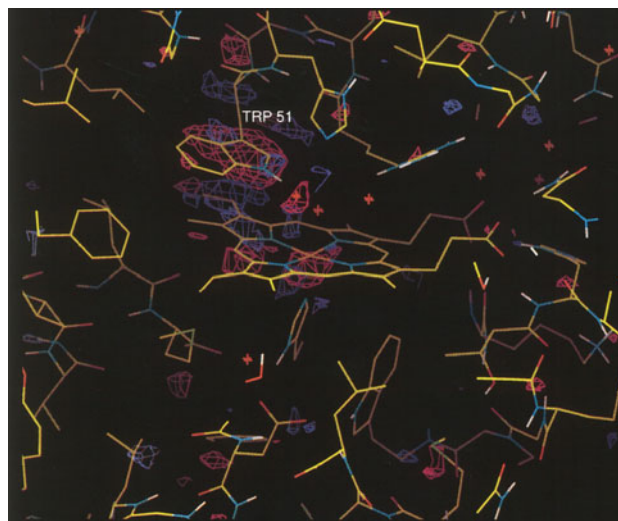
shift of $+22.5$ mV in phosphate buffer to a potential of -30 mV in BTP/MES; this latter is in much better agreement with the calculated value of -48 mV, and thus, we assign the discrepancy in the model noted above to some modality of phosphate binding—either in the distal pocket with an electrostatic influence or as a partly liganding species. For H52A, however, there is essentially no buffer effect—there is no difference in potential measured in phosphate or BTP/MES systems. A non-pH-dependent and lower midpoint potential can be generated by the addition of a sixth ligand. Two are explored here. Figure 2g shows titrations of CCP proteins with bound azide or fluoride [11, 25]. Table 1 shows midpoint potentials shifted ~ -30 mV by azide and ~ -83 mV by fluoride. Structural data for azide binding were adduced; Fig. 9 shows a $|2Fo| - |Fc|$ difference Fourier map with azide bound and a partly refined structure; evidence for a main and secondary binding site are observed (or alternatively, a binding site and an additional non-azide solvent species). The shape of the density and geometry of the heme/azide for the primary site is very similar to those seen for azide-bound ferric sea hare Mb (PDB structure 5MBA) and azide-bound ferric sperm whale Mb (PDB structure 1SWM). Though there is no direct evidence, the magnitude of the lower redox potential, the absence of pH dependence, and the theoretical calculation, all point to the possibility of a sixth ligand in H52A CCP, or alternatively to a nearby bound anion—without an active pK_a in the examined pH range. The X-ray data are not sufficient to determine this to be the case; more sophisticated, low temperature methods or additional spectroscopic data would be needed to firmly establish that this is the case and the identity of any bound or liganding

Table 2 Results of PDLD calculations[a]

Protein	ΔV (total)	$\Delta\Delta V$ (CCP)	$\Delta\Delta V$ (Mb)	Shift in Eo (CCP)	Shift in Eo (Mb)
CCP	39.9	0	15	0	650.5
D235A	37.3	−2.6	12.4	−112.7	537.7
H52A	38.1	−1.8	13.2	−78.1	572.4
R48A	41.0	1.1	16.1	47.7	698.2
W191G	39.1	−0.8	14.2	−34.7	615.8
W51A	40.3	0.4	15.4	17.3	667.8
Myoglobin	24.9	−15.0	0	−650.5	0
V68N	26.2	−13.7	1.3	−594.1	56.4
V68E	29.5	−10.4	4.6	−451.0	199.5
V68D	28.9	−11.0	4.0	−477.0	173.5
CCP-MD	37.9	0		0.0	
H52A-MD	35.8	−2.1		−91.1	

[a] With the sign convention utilized here, a positive shift in V indicates stabilization of the cationic (ferric) form. MD = molecular dynamics averaged values. Energies in kcal/mole; Eo in mV
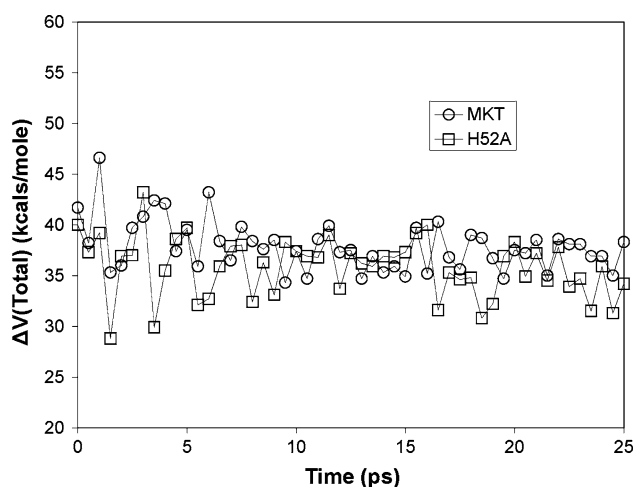

Fig. 8 Values of ΔV (Total) for H52A cytochrome *c* peroxidase and native (MKT) cytochrome *c* peroxidase over 25 p sec of molecular dynamics

species. An alternate hypothesis would be an altered picture of His-52 in the wild-type protein. The protonation scheme that the PDLD model derives and provides (see Sect. 2) may be incorrect; the proton may be on the other nitrogen, or in some mixed system (see e.g. [47]) or may participate in a complex with solvent water in the native system such that removal of His-52 results in net destabilization of the ferric form of the heme. Such system would presumably contain the origin of the pH dependence of the redox potential in CCP, such that its disruption by removal of His-52 leads to loss of said pH dependence. We note that the cavity itself in H52A is not solely responsible for this consequence; H52Q has essentially the same potential as H52A (and likewise, W191S and W51F afford the same analysis).

The relationship between spectral properties, spin/coordination state, and redox potential for CCP has been extensively reviewed by Erman and coworkers [9, 10] for a different set of mutants. (One mutant is the same—the potential for H52Q reported there is essentially identical to that reported here.) The published literature cited for the mutants under study here also discusses the analysis of these mutants by UV–Vis spectroscopy, by other methods, and the resulting conclusions about spin and coordination state. Most fall into the category of exhibiting mixed five and six coordinate and mixed high spin and low spin states. For H52A, the protein exhibits pH independent UV–Vis spectra which resemble that of yeast CCP at pH 6—and thus point to a five-coordinate high spin system for both ferric and ferrous forms. One cannot exclude from the UV–Vis data alone, however, the absence of some six coordinate high spin or six coordinate low spin content.

The use of sixth ligands to some extent can possibly create a "purer" system if the goal is just to study the electrostatics at the heme. The formal charge of the pair is also altered by this strategy (and depending on the physics goals—this could be desirable or undesirable). The azide or fluoride (or other such systems lacking pH dependence) may prove of value here. For CCP, the mutant H175G also affords in principle the ability to examine and control both proximal and distal ligands and to reach outside the structural menu of natural amino acids. We present here only an initial data set of redox potential data for H175G. Data are only available in phosphate buffer, and as noted this is known to have an impact in some H175G settings [20, 21]. For H175G, the so-called Green Form [38] at pH 7 has a midpoint potential of −127 mV, for the Red Form [38] at pH 6, it is −135.2 mV. H175G with bound imidazole and at pH 7.2 has a potential of −160 mV; not so very different from wild-type CCP; the slight upward shift tempts one to compare the data to D235N [17] and to focus on some disruption of the Triad, but more data are needed to reliably inform on these aspects. An azide-bound form (H175G with imidazole and azide, pH 7.20) exhibits a

Fig. 9 Cross-eyed stereo pair of $2|Fo| - |Fc|$ electron density maps for azide bound to CCP, contoured at 1σ, and superposed on the structure of native CCP (MKT). Density fitting an azide moiety exists above the heme and pointed toward the D ring in the protoporphyrin IX. Additional density near W51 and above ring A could represent a second binding site or a new, bound solvent species such as a small cation
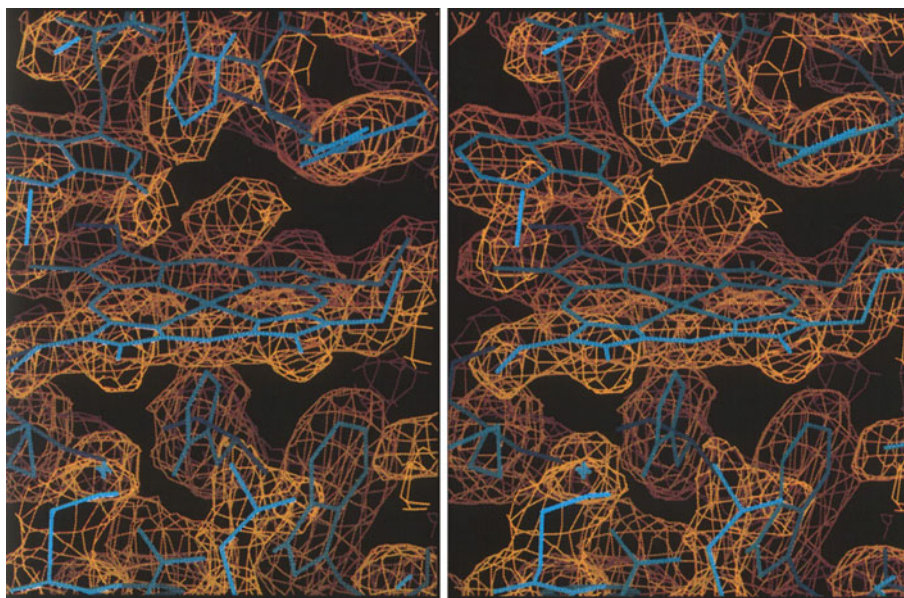
midpoint potential of -183.4 mV; the shift on azide binding is approximately the same as that for native CCP.

There are sources of uncertainty in both the experimental and theoretical elements at play in this study. We have seen buffer composition play a role, and we have seen some variation in the value of the Nernst slope; the theoretical treatments use only water (as Langevin dipoles) and assume a pure transition from a formally neutral five-coordinate ferrous CCP to a formally positive five-coordinate ferric CCP. We do no modeling of the changes to the liganding His-175. The readers should consult the cited literature on the mutants for data on the nature of the heme in each system, which is usually more complex/mixed. Errors in the calculations presented here are expected to be significant, but are reduced in significance substantially by the problem posed (comparing electrostatic stabilization of a species in very similar environments; see discussion in [28]).

References

1. Bonagura CA, Bhaskar B, Shimizu H, Li H, Sundaramoorthy M, McRee DE, Goodin DB, Poulos TL (2003) Biochemistry 42:5600–5608
2. Brünger AT, Kuriyan J, Karplus M (1987) Science 235:458–460
3. Bunte SW, Jensen GM, McNesby KL, Goodin DB, Chabalowski CF, Nieminen SRM, Suhai S, Jalkanen KJ (2001) Chem Phys 265:13–25
4. Cao Y, Goodin DB, McRee DE (1996) Acta Crystallographica Sect A A52:C130, PS04.02.14
5. Churg A, Warshel A (1986) Biochemistry 25:1675–1681
6. Conroy CW, Tyma P, Daum PH, Erman JE (1978) Biochim Biophys Acta 537:62–69
7. Cutler RL, Davies AM, Creighton S, Warshel A, Moore GR, Smith M, Mauk AG (1989) Biochemistry 28:3188–3197
8. Dawson JH (1988) Science 246:433–439
9. DiCarlo CM, Vitello LB, Erman J (2007) ECT Trans 6:27–45
10. DiCarlo CM, Vitello LB, Erman J (2007) J Inorg Biochem 101:603–613
11. Edwards SL, Poulos TL (1990) J Biol Chem 265:2588–2595
12. Erman JE, Vitello LB, Mauro JM, Kraut J (1989) Biochemistry 28:7992–7995
13. Fitzgerald MM, Churchill MJ, McRee DE, Goodin DB (1994) Biochemistry 33:3807–3818
14. Fitzgerald MM, Trester ML, Jensen GM, McRee DE, Goodin DB (1995) Protein Sci 4:1844–1850
15. Fitzgerald MM, Musah RA, McRee DE, Goodin DB (1996) Nat Struct Biol 3:626–631
16. Goodin DB, Davidson MG, Roe JA, Mauk AG, Smith M (1991) Biochemistry 30:4953–4962
17. Goodin DB, McRee DE (1993) Biochemistry 32:3313–3324
18. Goodin DB (1996) J Biol Inorg Chem 1:360–363
19. Hirst J, Goodin DB (2000) J Biol Chem 275:8582–8591
20. Hirst J, Wilcox SK, Williams PA, Blankenship J, McRee DE, Goodin DB (2001) Biochemistry 40:1265–1273
21. Hirst J, Wilcox SK, Ai J, Moénne-Loccoz P, Loehr TM, Goodin DB (2001) Biochemistry 40:1274–1283
22. Houseman ALP, Doan PE, Goodin DB, Hoffman BM (1993) Biochemistry 32:4430–4443
23. Howard AJ, Nielson C, Xuong NH (1985) In: Wyckoff HW, Hirs CHW, Timasheff SN (eds) Methods in enzymology, vol 114. Academic Press, Orlando, pp 452–472
24. Huyett JE, Doan PE, Gurbriel R, Houseman ALP, Sivaraja M, Goodin DB, Hoffman BM (1995) J Am Chem Soc 117:9033–9041
25. Jacobson T, Williamson J, Wasilewski A, Felesik J, Vitello LB, Erman JE (2004) Arch Biochem Biophys 422:125–136

26. Jalkanen KJ, Wuertz-Juergensen V, Claussen A, Rahim A, Jensen GM, Wade RC, Nardi F, Jung C, Degtyarenko IM, Nieminen RM, Herrmann F, Knapp-Mohammady M, Niehaus TA, Frimand K, Suhai S (2006) Int J Quantum Chem 106:1160–1198
27. Jensen GM, Goodin DB, Bunte SW (1996) J Phys Chem 100:954–959
28. Jensen GM, Bunte SW, Warshel A, Goodin DB (1998) J Phys Chem 102:8221–8228
29. Jensen GM, Warshel A, Stephens PJ (1994) Biochemistry 33:10911–10924
30. Jensen GM (1994) Ph.D. Dissertation, University of Southern California
31. Kassner RJ (1972) Proc Natl Acad Sci USA 69:2263–2267
32. Kassner RJ (1973) J Am Chem Soc 95:2674–2677
33. Langen R, Brayer GD, Berghuis AM, McLendon G, Sherman F, Warshel A (1992) J Mol Biol 224:589–600
34. Langen R, Jensen GM, Jacob U, Stephens PJ, Warshel A (1992) J Biol Chem 267:25625–25627
35. Lee FS, Zhen-Tao C, Bolger MB, Warshel A (1992) Protein Eng 5:215–228
36. Liu K, Williams J, Lee H, Fitzgerald MM, Jensen GM, Goodin D, McDermott A (1998) J Am Chem Soc 120:10199–10202
37. McRee DE (1992) J Mol Graph 10:44–46
38. McRee DE, Jensen GM, Fitzgerald MM, Siegel HA, Goodin DB (1994) Proc Natl Acad Sci USA 91:12847–12851
39. Musah R, Goodin DB (1997) Biochemistry 36:11665–11674
40. Musah RA, Jensen GM, Rosenfeld RJ, McRee DE, Goodin DB, Bunte SW (1997) J Am Chem Soc 119:9083–9084
41. Musah RA, Jensen GM, Bunte SW, Rosenfeld RJ, Goodin DB (2002) J Mol Biol 315:845–857
42. Nicola NA, Minasian E, Appleby CA, Leach SJ (1975) Biochemistry 14:5141–5149
43. Nigro AP, Goodin DB (2010) Arch Biochem Biophys 500:66–73
44. Parson WW, Chu ZT, Warshel A (1990) Biochim Biophys Acta 1017:251–272
45. Poulos TL (1988) Adv Inorg Biochem 7:1–33
46. Rees DC, Farrelly D (1990) In: Sigman DS, Boyer PD (eds) The enzymes, vol 19. Academic Press, San Diego, pp 37–97
47. Satterlee JD, Alam SL, Mauro JM, Erman JE, Poulos TL (1994) Eur J Biochem 224:81–87
48. Scholes CP, Liu Y, Fishel LA, Farnum MF, Mauro JM, Kraut J (1989) Isr J Chem 29:85–92
49. Sivaraja M, Goodin DB, Smith M, Hoffman BM (1989) Science 245:738–740
50. Stankovich MT (1980) Anal Biochem 109:295–308
51. Stephens PJ, Jollie DR, Warshel A (1996) Chem Rev 96:2491–2513
52. Sun J, Fitzgerald MM, Goodin DB, Loehr TM (1997) J Am Chem Soc 119:2064–2065
53. Varadarajan R, Zewert T, Gray HB, Boxer SG (1989) Science 243:69–72
54. Wang JM, Mauro JM, Edwards SL, Oatley SJ, Fishel LA, Ashford VA, Xuong NH, Kraut J (1990) J Biol Chem 265:2588–2595
55. Warshel A (1991) Computer modeling of chemical reactions in enzymes and solutions. Wiley, New York
56. Wilcox SK, Jensen GM, Fitzgerald MM, McRee DE, Goodin DB (1996) Biochemistry 35:4858–4866
57. Zhou H-X (1994) J Am Chem Soc 116:10362–10375